Indian Journal of Engineering & Materials Sciences
Vol. 30, June 2023, pp. 452-459
10.56042/ijems.v30i3.3701

Study on the Effect of UV Exposure on WO_3/PVA based Nanocomposite Films

Jaspreet Kaur[a], Navneet Kaur[a], Savita[a], Tripti Gupta[b], R P Chauhan[b], & Annu Sharma[a*]

[a]Department of Physics, Kurukshetra University, Kurukshetra 136 119, India

[b]National Institute of Technology, Kurukshetra 136 119, India

Received: 10 May 2023; Accepted: 31 May 2023

In the present work, Polyvinyl Alcohol (PVA) polymer has been chosen as a host matrix to incorporate tungsten trioxide (WO_3) nanofillers for synthesizing self-supporting and flexible nanocomposites (NCs). WO_3 has been synthesized using the hydrothermal treatment and subsequently WO_3/PVA based NCs were prepared via solution casting technique. To ascertain the morphology and structure of fabricated NCs, scanning electron microscopy (SEM) and X-Ray Diffraction (XRD) techniques were used. Further, XRD data has been analyzed to calculate the crystallite size (nm) of WO_3 powder. The SEM micrograph depicts the rod-like morphology of the prepared sample. The optical parameters like band gap (E_g), refractive index (n), and optical conductivity (σ_{opt}) of prepared NCs were computed using optical data. Transmittance (%) of prepared NCs has been found to decrease with increasing wt% of WO_3 in PVA in UV regime highlighting their potential application in UV shielding devices. To study the effect of UV exposure on prepared NCs, optical spectroscopy has been used in diffuse reflectance (%) mode. The prepared NCs exhibit a significant decrease in diffuse reflectance (%) with increasing UV exposure time. Coloration efficiency (η_{ph}) of the WO_3/PVA NCs has been calculated using optical data. Coloration efficiency (η_{ph}) of 10 wt% WO_3/PVA NC film is (~ 0.1099) and decreases with a decrease in wt% of WO_3 in PVA.

Keywords: Hydrothermal Treatment, Nanocomposite (NC) Film, Crystallite Size (nm), Band Gap (E_g), Refractive Index (n), Optical Conductivity (σ_{opt}), and Coloration Efficiency (η_{ph})

1 Introduction

The phenomenon of photochromism usually refers to a continuous and reversible transformation in absorption spectra/electrical conductivity/ fluorescence emission exhibited by a chemical species on exposure to UV radiation[1]. Such photochromic materials have applications in many disciplines such as the textile industry[2], digital information storage[3], smart windows[4], rewritable media[5], molecular switches[6], multi-photonic devices[7], optoelectronic devices[8], etc. Till now, several organic materials such as diarylethene and azobenzene as well as inorganic materials such as rare earth complexes, transition metal oxides (TMOs), and metal halides have been explored to study their behavior in terms of color transition and optical performance under the effect of UV exposure makes them a potential candidate to be used as 'smart windows'. However, inorganic substances are usually preferred over organic substances as they show better color contrast and fast coloring/bleaching rates[9-12]. Among various inorganic photochromic materials, tungsten trioxide (WO_3) is being explored extensively by researchers as it changes its color substantially under the effect of external stimuli. However, some bottlenecks such as long bleaching time, poor photochromic response, and low photoresponse kinetics exist. To overcome such bottlenecks, several strategies such as size and morphology optimization, fast generation/ transportation of charge carriers, combining with other transparent semiconductors, and using hydrogen bond-rich matrix have been adopted[13-16]. Dispersion of WO_3 in an appropriate polymer matrix such as polyvinyl pyrollidone (PVP), polyethylene glycol (PEG), polyvinyl pyrollidone/polyurethane, etc. which are good proton donors is an effective strategy for improving its performance. Hidetoshi Miyazaki et. al synthesized a WO_3-urethane matrix and demonstrated that with the decrease in film thickness, coloring speed increases while bleaching speed decreases[17]. Rong Li et. al synthesized WO_3-PVP/PU nanocomposite and concluded that by selecting the proper proportion of the polymer matrix, coloring and bleaching processes can be modulated[13]. Yong Zhu et.al synthesized PVA-WQD (tungsten quantum dot) nanocomposite films using ethylene glycol. The fabricated nanocomposite films displayed a fast photo response speed (90%)[1]. However, to the best of our

*Corresponding author (E-mail: asharma@kuk.ac.in)

knowledge, limited studies are available on the photochromic response of WO_3 nanorods in PVA polymer matrix with varying concentrations of WO_3 and changing UV exposure time. Thus in the present work, an attempt has been made to investigate the photochromic response of WO_3 nanorods prepared using hydrothermal treatment when embedded in a PVA matrix. Moreover, the effect of increasing wt% of WO_3 nanorods in a PVA matrix with varying UV exposure times was studied. The in-depth structural, optical, and photochromic behavior of NC films was accomplished using various characterization techniques such as XRD, SEM, and UV-Vis spectroscopy.

2 Materials and Methods

2.1 Chemicals Used

Thioacetamide (TAA, ≥99%), Sodium tungstate dihydrate ($Na_2WO_4.2H_2O$, ≥99.5%), and Hydrochloric Acid (HCl, ≥95%) were procured from HiMedia. Oxalic Acid ($C_2H_2O_4$, ≥99%) and PVA (Polyvinyl alcohol) were purchased from Rankem, India.

2.2 Method of synthesis

2.2.1 Synthesis of WO_3

WO_3 powder was synthesized using hydrothermal treatment as depicted in Fig. 1 (a). Firstly, 1.2 g $Na_2WO_4.2H_2O$ and 1.6 g TAA were dissolved in 80 ml deionized (DI) water under continuous magnetic stirring at 50 °C for 1.5 h. After 30 min, 0.6 g oxalic acid was added to the solution. After that HCl was added dropwise to adjust the pH at 1. Then, the solution was transferred to a 100 ml Teflon container in an autoclave and kept for 24 h at 180 °C in a muffle furnace. On cooling to room temperature, the autoclave was opened and precipitates were collected and washed several times with DI water and absolute ethanol. The resultant suspension was centrifuged at 6000 rpm for 20 min. Finally, obtained sample was kept at 80 °C for 12 h in the oven and annealed at 400 °C for 3 h.

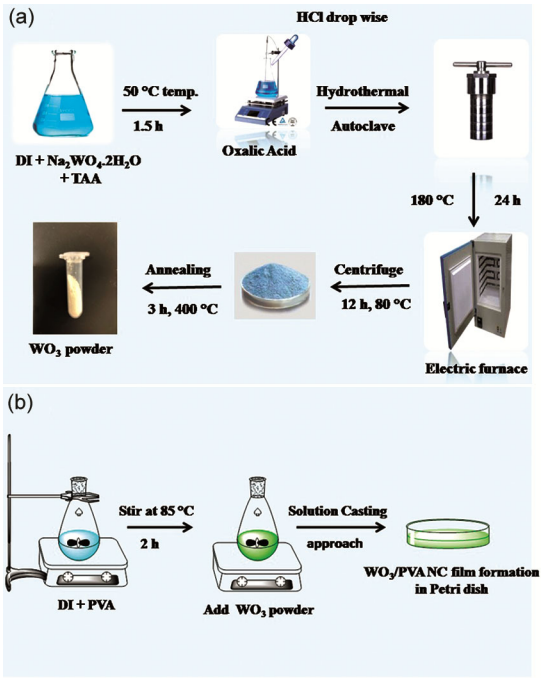

Fig. 1 — Block diagram (a) of hydrothermal synthesis of WO_3 powder and (b) WO_3/PVA NCs via solution casting approach.

2.2.2 Synthesis of WO_3/PVA NCs

For preparing NCs, a solution casting approach was employed as depicted in Fig. 1 (b). To synthesize PVA film, 1g of PVA was dispersed in 20 ml of DI water under continuous magnetic stirring at 85 °C for 2 h. The same procedure was carried out with the addition of different concentrations (1 wt%, 5 wt%, 10 wt%) of WO_3 powder and finally, suspensions were transferred to the different Petri dishes. On drying under dark conditions, films were peeled off for further characterization. The thickness of the fabricated NCs was ascertained using a screw gauge and comes out to be 210 $\pm$ 2.6 µm. The percentage weight fraction (wt%) of WO_3 was calculated using eq. 1 :

$$wt\% = \frac{w_f \times 100}{w_f + w_p} \quad \ldots (1)$$

where w_f is the weight of WO_3 and w_p is the weight of PVA.

2.2.3 Characterizations

For structural characterization of the synthesized powder and NCs, X-ray diffraction measurements (XRD) were carried out by using X-Ray Bruker D8 Advance Diffractometer by employing Cu-K_α radiation in the 2θ range (10°-80°). To ascertain the morphology of WO_3 powder, Scanning Electron Microscope (JOEL JSM-6390 LV) device was used. To investigate the optical and photochromic properties of prepared NCs, "Shimadzu UV-VIS-NIR Spectrophotometer UV-3600 Plus" apparatus was used in the 200 nm to 800 nm wavelength range.

3 Results and Discussion

3.1 SEM

The surface morphology of the hydrothermally synthesized WO_3 powder was examined by SEM. The

SEM image (Fig. 2 (a)) reveals the rod-like morphology of prepared WO_3. The image further discloses that nanorods exhibit clear and smooth surfaces. The average diameter of nanorods comes out to be 70.18 ± 1.2 nm whereas the length of nanorods scaled up to a few hundred nm. To corroborate the chemical composition of WO_3, the prepared sample was analyzed using Energy-dispersive X-rays spectroscopy (EDAX), and the results are depicted in Fig. 2 (b). The average weight percentage of W and O is found to be 74.89 and 25.11, respectively, indicating almost 1:3 stoichiometry[18] for element W to O as presented in Fig. 2 (b).

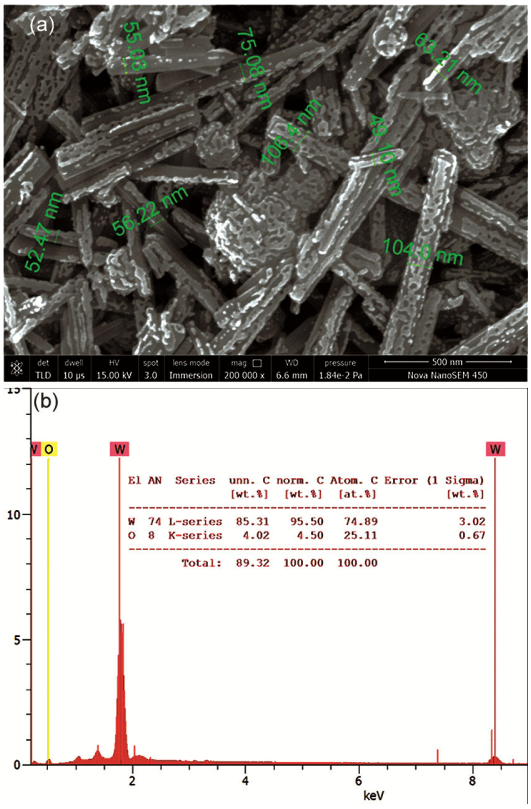

Fig. 2 — (a) SEM image and (b) EDAX of WO_3 powder with the distribution of weight% and atomic% of elements W and O.

3.2 XRD analysis

Figure 3 (a) depicts the XRD pattern of WO_3 powder synthesized via hydrothermal treatment. The observed diffraction peaks are indexed and match well with the data present in JCPDS File No. 75-2187. The diffraction peaks are sharp and narrow indicating the crystalline hexagonal phase, thus confirming the formation of h-WO_3 with space group P6/mmm and lattice parameters a & b = 0.7298 nm, c = 0.3899 nm[18]. Figure 3 (b) depicts the XRD pattern of PVA and WO_3/PVA NCs with increasing wt% of WO_3. In the XRD pattern of PVA, a prominent peak at 2θ position of 20.7° was observed[19]. XRD pattern of WO_3/PVA NCs reveals that the intensity of diffraction peaks of PVA decreases while that of WO_3 increases with increasing concentration of WO_3 nanorods. Further, XRD data was analyzed to calculate the crystallite size 'D' of the WO_3 powder which comes out to be 27.649 nm using Debye-Scherrer formula given in eq. 2:

$$D = \frac{k\lambda}{\beta \cos\theta} \quad \ldots (2)$$

where k = 0.9 (Scherrer constant), β is full width at half maximum (FWHM) of the most intense peak, present at 2θ = 27.8° in the present case, λ=0.15418 nm is the wavelength[19].

The interplanar spacing (d) corresponding to the most intense peak (2θ = 27.8°) was calculated using eq. 3 and values are listed in table 1.

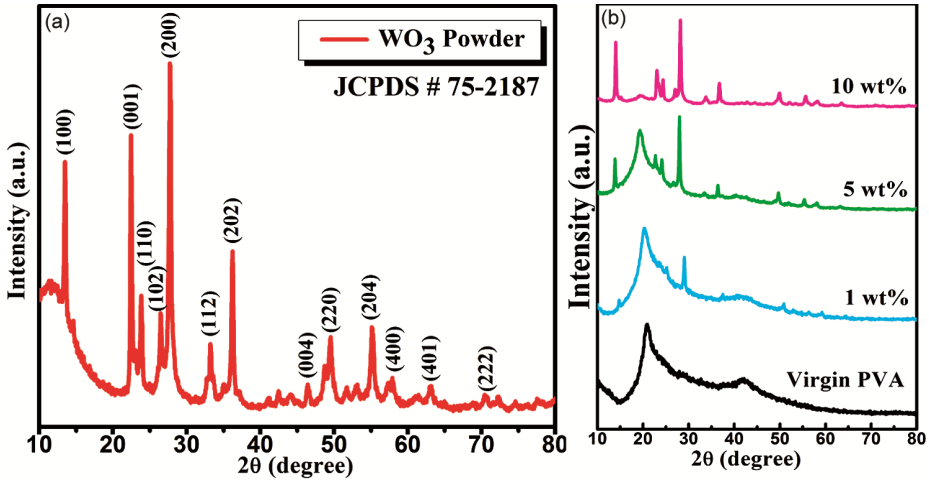

Fig. 3 — XRD pattern of (a) WO_3 powder, (b) PVA, and WO_3/PVA NCs with increasing wt% of WO_3.

$$\frac{1}{d^2}=\frac{4}{3}\left(\frac{h^2+K^2+hk}{a^2}\right)=\frac{\iota^2}{c^2} \quad \ldots(3)$$

Further, dislocation density (δ) and microstructural strain[20] induced (ε) in the PVA matrix on the incorporation of nanofiller was calculated using eq. 4 and 5:

$$\delta=\frac{1}{D^2} \quad \ldots(4)$$

$$\varepsilon=(\beta)/4\ tan\theta \quad \ldots(5)$$

3.3 Optical studies

3.3.1 UV-Vis absorption spectra

Figure 4 (A) presents the UV-Vis absorption spectra of PVA and WO_3/PVA NCs. In Fig. 4 (A), the spectra of PVA display its signature absorption band at 278 nm which can be ascribed to π→π* electronic transition type arising because of unsaturated bonds (C=O and C=C)[21]. Absorption spectra of 1wt% WO_3/PVA NC film show an absorption band edge at around 400 nm which shifts to higher wavelengths with increasing wt% of WO_3 in the PVA matrix. Further, absorption data was utilized to determine the optical energy gap (E_g) of prepared NCs. E_g was estimated by Tauc relation[19] using eq. (6):

$$(\alpha h\nu)^{\frac{1}{2}}=C_o(h\nu-E_g) \quad \ldots(6)$$

where 'hν' is the photon energy, C_o is a constant and 'α' is the absorption coefficient and is given by eq. 7:

$$\alpha=\frac{2.303\times Abs}{x} \quad \ldots(7)$$

where Abs is the absorbance and x is the thickness of the NC film[19].For calculating E_g of NCs, a graph between $(\alpha h\nu)^{1/2}$ and hν (eV) was plotted and is presented in Fig. 4 (B). By extrapolating the linear fitted line to hν axis (such that α=0), E_g was calculated and values are given in table 1 for PVA and WO_3/PVA NCs.The value of E_g for PVA comes out to be 4.83 ± 0.16 eV and decreases to 2.44 ± 0.06 eV for 10 wt% WO_3/PVA NC.

This decrease in the value of E_g for PVA on addition of increasing wt% of WO_3 may be attributed to the formation of defects in the form of trapping and recombination centres within the region of HOMO-LUMO (Highest Occupied Molecular Orbital - Lowest Unoccupied Molecular Orbital) gap of host matrix[22].

3.3.2 Transmission and Reflectance spectra

Figure 4 (c) represents the transmittance spectra of PVA and WO_3/PVA NCs. The transmission intensity of PVA is about 84% over the entire visible region and decreases to 20% for 10 wt% of WO_3/PVA NC film. Further, the transmittance intensity of the NC

Table 1 — Different crystallographic parameters corresponding to WO_3/PVA NCs.

Sample	Crystallite size (D) (nm)	Dislocation density (δ) (10^{15}lines/m^2)	Strain (ε)
1 wt%	17.82	3.149	0.1126
5 wt%	25.36	1.55	0.3210
10 wt%	25.02	1.59	0.3236

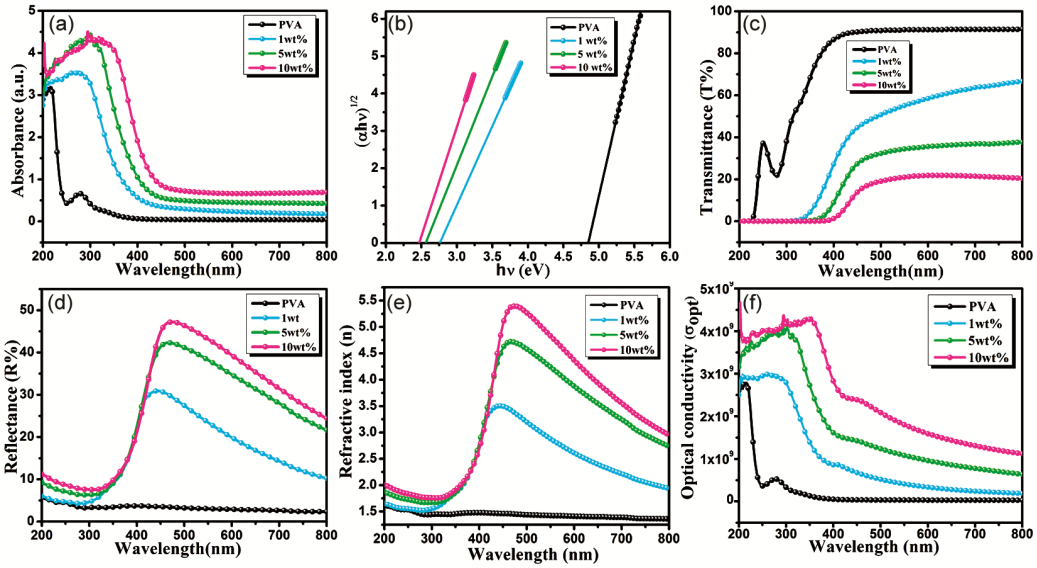

Fig. 4 — (a) UV-Vis absorption spectra, (b) Plot of $(\alpha h\nu)^{1/2}$ versus hν (eV), (c) Transmittance spectra, (d) Reflectance spectra, (e) Variation of refractive index, (f) optical conductivity of PVA and WO_3/PVA NCs.

Table 2 — Values of E_g and Transmittance (%) corresponding to PVA and WO_3/PVA NCs.

Sr. No.	Sample	Optical Energy Gap E_g (eV)	Transmittance (%) in the UV region
1.	PVA	4.83 ± 0.16	40
2.	1 wt% WO_3/PVA NC	2.71 ± 0.09	0.15
3.	5 wt% WO_3/PVA NC	2.52 ± 0.08	0.04
4.	10 wt% WO_3/PVA NC	2.44 ± 0.06	0.01

decreases significantly in the region 200-400 nm (UV region) with the addition of WO_3, and results are listed in table 2. Thus prepared WO_3/PVA NCs have the capability of blocking the UV region and can serve as a potential candidate to be used in UV blocker devices. Figure 4 (d) presents the variation of reflectance of PVA with increasing wt% of WO_3 and it is clear that reflectance increases with increasing wt% of WO_3 in the PVA matrix.

3.3.3 Refractive index (n) and optical conductivity (σ_{opt})

The variation of refractive index (n) with wavelength (nm) for PVA and WO_3/PVA NCs is shown in Fig. 4 (e). Refractive index of a material is a vital parameter as it determines its applications in optical fiber communication systems and can be calculated using absorption and reflectance data. To calculate the refractive index[19] (n) of NCs, eq. 8 was used:

$$n = \frac{(1+R) + \sqrt{4R - (1-R)^2 K^2}}{(1-R)} \quad \ldots(8)$$

where 'R' stands for reflectance and 'K' stands for extinction coefficient[19] and is given by eq. 9:

$$K = \frac{a\lambda}{4\pi} \quad \ldots(9)$$

Figure 4 (E) shows that refractive index (n) increases significantly with increasing wt% of WO_3 in the PVA matrix and it increases from 1.4 for PVA to 3.3, 4.7, and finally 5.3 for 1 wt%, 5 wt%, and 10 wt% WO_3/PVA NCs respectively at 475 nm. Such a significant increase in the value of the refractive index (n) of PVA on the incorporation of WO_3 may be accredited to some recombination and trapping centers created within the HOMO-LUMO gap of the host matrix[23]. Further, refractive index (n) and absorption coefficient were utilized to calculate optical conductivity[19] (σ_{opt}) of fabricated NCs by using eq. 10:

$$\sigma_{opt} = \frac{\alpha n c}{4\pi} \quad \ldots(10)$$

where 'c' stands for the velocity of light.

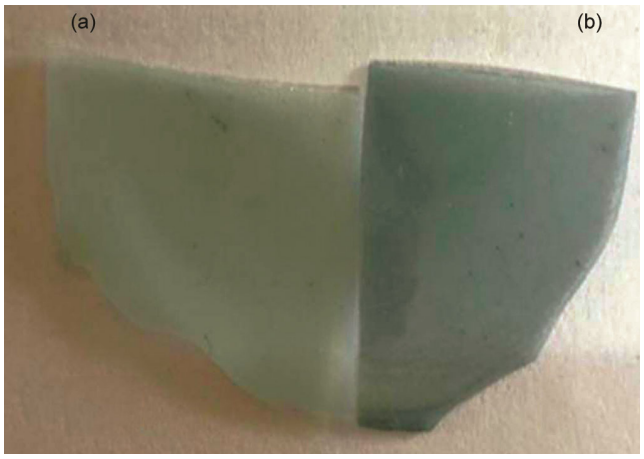

Fig. 5 — Digital photograph of 1wt% WO_3/PVA NC film showing the color variation before (a), and after (b) UV exposure.

Figure 4 (f) represents the variation of optical conductivity (σ_{opt}) with wavelength (nm) of PVA with increasing wt% of WO_3. From Fig. 4 (f), it can be discerned that optical conductivity increases appreciably with increasing wt% of WO_3 in the PVA matrix which may be due to the creation of localized sites within the HOMO-LUMO gap of the host matrix which in turn increases the possibility of transitions[19].

3.4 Photochromic studies

The effect of increasing wt% of WO_3 on the photochromic behavior of WO_3/PVA NCs when subjected to changing UV exposure time was studied using UV-Vis spectroscopy in reflectance (%) mode in the region 200-800 nm. Fig. 5 (a) illustrates that the color of WO_3/PVA NC film changes from green to blue upon UV exposure.

Further, the variation in reflectance with increasing UV exposure time and increasing wt% of WO_3 in PVA matrix was studied. The NCs embedded with WO_3 in the PVA matrix were irradiated with UV radiations for varying time intervals (i.e. 20, 40, and 60 minutes) and variations in reflectance (%) are shown in Fig. 6 (a) to (c). Figure 6 (a-c) displays that on UV irradiation the reflectance of all the WO_3/PVA NCs decreases. Further, it was noticed that the decrease in reflectance becomes more prominent with the increase in exposure time. Figure 6 (d) depicts the variation in reflectance (R%) vs exposure time for WO_3/PVA NCs. It was observed that maximum variation in reflectance on UV exposure was exhibited by 10 wt% WO_3/PVA NC film. When WO_3/PVA NCs are exposed to UV radiation, electrons in the V.B (valence band) get excited to the C.B (conduction band) leading to the formation of a number of

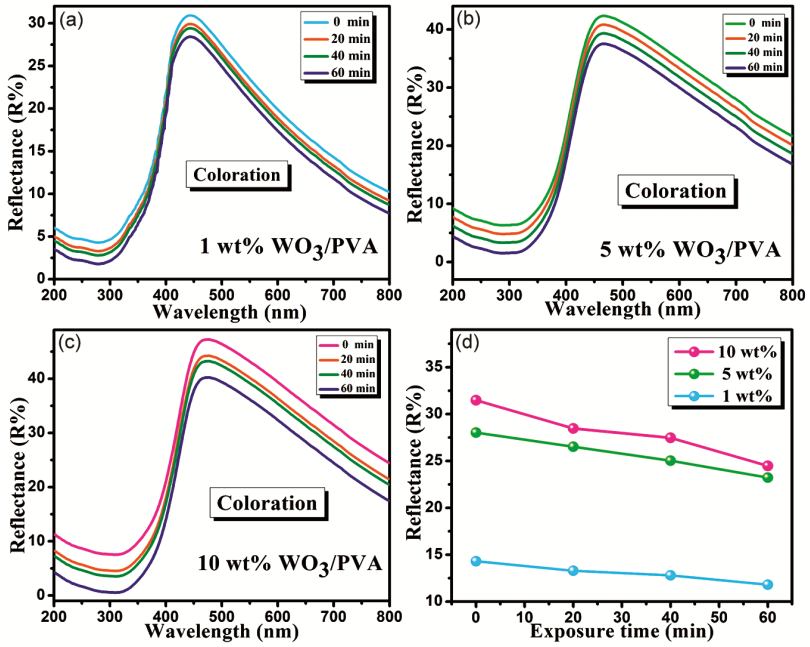

Fig. 6 — Reflectance (R%) of WO_3/PVA NCs before and after UV exposure with changing UV exposure time of (a) 1wt%, (b) 5wt%, (c) 10wt% respectively, and (d) the variation of reflectance (R%) with changing exposure time for WO_3/PVA NCs at 700 nm.

electron-hole pairs. Simultaneously, the PVA matrix acts as an effective proton donor with a large number of hydroxyl ions[24]. The photogenerated holes accelerate the proton propagation by reacting with structural H_2O molecules through hydrogen bonding to generate H^+ and highly reactive oxygen radical[1]. Subsequently, the cations occupy the position of oxygen vacancies to form metastable tungsten bronze (H_xWO_3)[25]. Thus the reduction of W ions from +6 to +5 upon UV illumination, acts as a blue color state which can be accredited to the intervalence charge transfer (IVCT)[26] of electrons between the W^{6+} to W^{5+}. Thus, synthesized homogeneous WO_3/PVA NCs facilitate proton intercalation that significantly enhances the coloration process.

Moreover, the coloration efficiency (η_{ph})[27] of the WO_3/PVA NCs was determined using eq. 11:

$$\eta_{ph} = \frac{\Delta OD}{It} \quad \ldots(11)$$

where, 'ΔOD' is the change in the optical density and 't' is the exposure time.

The change in the optical density (ΔOD) was calculated using eq. 12:

$$\Delta OD = \log_{10}\left(\frac{R_{BUV}}{R_{AUV}}\right) \quad \ldots(12)$$

Where, R_{BUV} and R_{AUV} are the reflectance (R%) before and after UV exposure, respectively.

Table 3 — Relative Reflectance (RR%) and coloration efficiency of WO_3/PVA NCs at 700 nm after 60 min of UV exposure.

Sample	Reflectance at 700 nm of NCs (BUV)	Reflectance at 700 nm of NCs (AUV)	Relative reflectance (RR%)	Coloration Efficiency $\eta_{ph} \propto \Delta OD$
1 wt%	14.299	11.799	17.7%	0.0849
5 wt%	28.023	23.223	18.3%	0.0878
10 wt%	31.471	24.471	22.3%	0.1099

Table 3 summarizes the relative reflectance (RR%) values and η_{ph} of WO_3/PVA NCs under the effect of UV exposure for 60 min. at 700 nm. It was observed that (RR%) and η_{ph} displayed by NCs depends on concentration and varies directly with the concentration of WO_3 in PVA i.e. with increasing concentration of the WO_3 nanofiller in the PVA matrix, (RR%) also increases. It was clear that the specimen with 10 wt% of WO_3 in the PVA matrix shows the maximum coloration efficiency (~ 0.1099) as well as (RR%) value (~ 22.3). Besides coloring behavior, the bleaching process of the fabricated photochromic films also plays a vital role in determining their potential applications in smart windows. Therefore, an in-depth analysis was carried out to understand the bleaching process. The variation in reflectance for each WO_3/PVA NC film corresponding to 60 min. of UV exposure for the bleaching process was recorded at different intervals and the results are presented in Fig. 7 (a), (b), and (c).

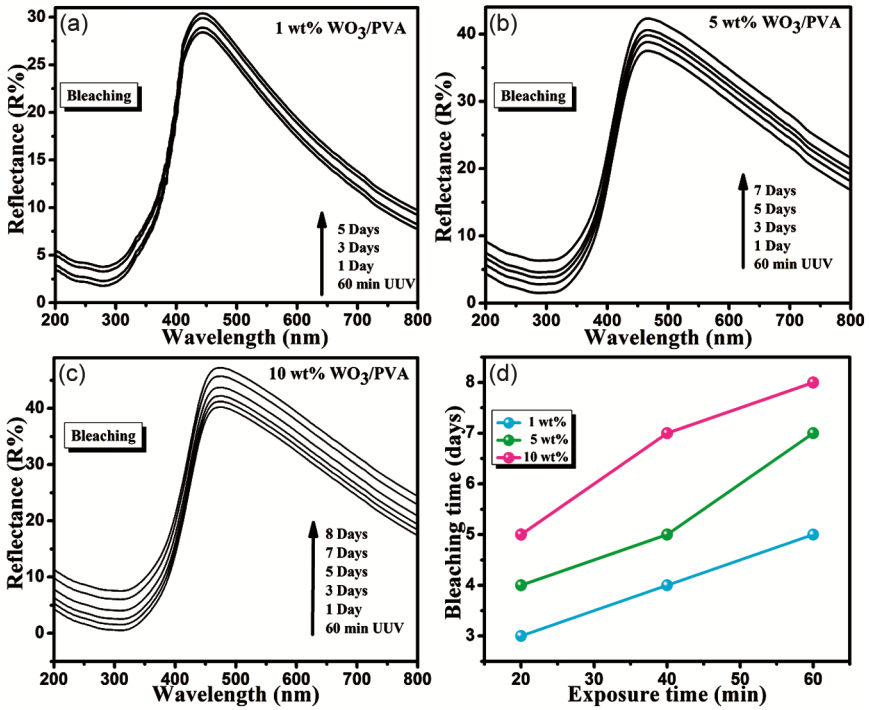

Fig. 7 — Variation in reflectance (R%) of (a) 1wt%, (b) 5wt%, and (c) 10wt% WO_3/PVA NCs corresponding to 60 min. of UV exposure recorded for bleaching process at different intervals of time (d) variation of bleaching time (days) versus exposure time (min) for each WO_3/PVA NC film.

It was found that like coloration, bleaching is also concentration and exposure time dependent. Broadly, the longer the exposure time, more is the bleaching time. Further, it was observed that bleaching time varies directly with the concentration of nanofillers in the matrix i.e. higher the concentration, more is the bleaching time.

It was found that PVA NC film with different wt% of WO_3 return to its original state after different intervals of time. It was found that higher-concentration film requires more time to bleach than low-concentration NC film which may be because high-concentration film has a low supply of combining H^+ ions which increases the bleaching time[28-29]. Figure 7 (d) represents the variation of bleaching time with exposure time for each WO_3/PVA NC film and it was observed that bleaching time shows almost direct variation with the exposure time.

4 Conclusion

1D WO_3 powder sample was synthesized successfully via hydrothermal treatment and subsequently used for the synthesis of WO_3/PVA NCs with varying wt% of WO_3 via solution casting approach. XRD confirms the hexagonal structure of WO_3 powder while FESEM depicts the rod-like morphology of the sample prepared via hydrothermal treatment. The average diameter of nanorods comes out to be 70.18 ± 1.2 nm whereas length varies in a few hundred nanometers. The value of E_g calculated for PVA comes out to be 4.83 ± 0.16 eV and decreases to 2.44 ±0.06 eV for 10 wt% WO_3/PVA NC film. Refractive index (n) increases significantly with increasing wt% of WO_3 in the PVA matrix and it increases from 1.4 for PVA to 5.3 for 10 wt% WO_3/PVA NC film. The optical transmittance (%) of WO_3/PVA NCs was found to decrease with increasing wt% of WO_3 and blocks UV region indicating their potential application as UV blockers. The photochromic response of WO_3/PVA NCs was studied with the effect of varying concentrations of nanofiller in the host matrix and varying UV exposure time. Photochromic studies reveal that 10 wt% WO_3/PVA NCs show the maximum optical modulation with high coloration efficiency (~ 0.1099) and (RR%) value (~ 22.3). corresponds. It was also found that NCs exposed to higher UV exposure time require more time to bleach. Further, it was observed that bleaching time increases with an increase in the wt% of WO_3 nanorods in the host matrix. The promising UV-blocking capacity and high flexibility

of prepared self-supported NCs make them sought-after materials for the fabrication of smart windows in energy-efficient buildings.

Acknowledgment

The authors are thankful to Ion Beam Center, Kurukshetra University, Kurukshetra, for providing XRD and UV-Vis spectroscopy facilities. The authors also acknowledge MNIT, Jaipur for providing SEM facility. One of the authors (JK) thanks RUSA for providing financial assistance.

References

1 Zhu Y, Yao Y, Chen Z, Zhang Z, Zhang P, Cheng Z & Gao Y, *Sol Energy Mater Sol Cells*, 239 (2022) 111664.
2 y M A, Joshi M & Butola B S, *J Eng Fibers Fab*, 9(1) (2014) 155892501400900113.
3 Wales D J, Cao Q, Kastner K, Karjalainen E, Newton G N & Sans V, *Adv Mater*, 30(26) (2018) 1800159.
4 Tällberg R, Jelle B P, Loonen R, Gao T & Hamdy M, *Sol Energy Mater Sol Cells*, 200 (2019) 109828.
5 Wei J, Jiao X, Wang T & Chen D, *ACS Appl Mater Interfaces,* 8(43) (2016) 29713.
6 Natali M & Giordani S, *Chem Soc Rev*, 41(10) (2012) 4010-4029. Irie M, *Pure Appl Chem,* 68(7) (1996) 1367.
7 Wang Q, Diez-Cabanes V, Dell'Elce S, Liscio A, Kobin B, Li H, Bredas J L, Hecht S, Palermo V, List-Kratochvil E J & Ligorio G, *ACS Appl Nano Mater*, 2(2) (2019) 1102.
8 Schulze M, Utecht M, Moldt T, Przyrembel D, C. Gahl, M. Weinelt, P. Saalfrank & Tegeder P, *Phys Chem Chem Phys,* 17(27) (2015) 18079.
9 Luo Q, Cheng H & Tian H, *Polym Chem*, 2(11) (2011) 2435-2443. Ejeromedoghene O, Oderinde O, Yao F, Akinremi C, Adewuyi S & Fu G, *Res Chem Intermed,* 47(9) (2021) 3807.
10 Egranov A V, Sizova T Y, Shendrik R Y & Smirnova N A, *J Phys Chem of Solids,* 90 (2016) 7.
11 Li R, Zhou Y, Shao Z, Zhao S, Chang T, Huang A, Li N, Ji S & Jin P, *ChemistrySelect,* 4(33) (2019) 9817.
12 Shen Y, Yan P, Yang Y, Hu F, Xiao Y, Pan L & Li Z, *J Alloys Compd,* 629 (2015) 27.
13 Quevedo-Lopez M A, Reidy R F, Orozco-Teran R A, Mendoza-Gonzalez O & Ramirez-Bon R, *J Mater Sci Mater Electron*, 11(2) (2000) 151.
14 Gavrilyuk A I, *Sol Energy Mater Sol Cells,* 94(3) (2010) 515.
15 Miyazaki H, Ishigaki T, Suzuki H &Ota T, *Bull Chem Soc Jpn,* 89(1) (2016) 20.
16 Wang H, Xu P & Wang T, *Mater des*, *23*(3) (2002) 331.
17 Durgesh, Kumar R, Sharma P K & Sharma A, *Mater Sci Eng B*, 276 (2022) 115560.
18 Morad I, Alshehri A M, Mansour, A F, Wasfy M H, & El-Desoky M M, Facile synthesis and comparative study for the optical performance of different TiO2 phases doped PVA nanocomposite films, *Physica B: Condens Matter,* 597, (2020) 412415.
19 Aziz S B, Abdullah O G, Hussein A M, Abdulwahid R T, Rasheed M A, Ahmed H M, Abdalqadir S W & Mohammed A R, *J Mater Sci Mater,* 28(10) (2017) 7473.
20 Kumar R, Kaushik R, Kumar R, Jose D A, Sharma P K & Sharma A, *Mater Chem Phys,* 260 (2021) 124132.
21 Meena & Sharma A, *Int J Polym Anal*, 26(5) (2021) 396.
22 Buslov D K, Sushko N I & Tretinnikov O N, *Polym Sci Ser A+*, 53(12) (2011) 1121.
23 Wei J, Jiao X, Wang T & Chen D, *ACS Appl Mater Interfaces,* 8(43) (2016) 29713.
24 Andron I, Marichez L, Jubera V, Labrugere C, Duttine M, Frayret C & Gaudon M, *ACS Appl Mater Interfaces,* 12(41) (2020) 46972.
25 Songara S, Gupta V, Patra M K, Singh J, Saini L, Gowd G S, Vadera S R & Kumar N, *J Phys Chem Solids,* 73(7) (2012) 851.
26 Yang Y, Guan L & Gao G, *ACS Appl Mater Interfaces,* 10(16) (2018) 13975.
27 Adachi K, Tokushige M, Omata K, Yamazaki S & Iwadate Y, *ACS Appl Mater Interfaces,* 8(22) (2016) 14019.